Computational Nanomaterials Design: towards the realization of nanoparticle use in radiotherapy Case Study 2: Adsorption states of At on Au(111) surface

Abstract

Astatine-211 (^{211}At) used as an α particle emitter is currently gaining as treatment method for cancer cells. It must however be attached to a carrier to facilitate the treatment process. Gold nanoparticle is a good candidate that has been used in several tests. Knowing the physics behind the adsorption of astatine on gold nanoparticles would be advantageous in designing a more optimal method for such applications. We therefore performed density functional theory calculation on astatine adsorption on gold (111) surface to understand both the mechanism of astatine bonding with gold and the strength of the bonding. We found the mechanism of adsorption to be the hybridization between the 6p orbital of astatine and the 5d and 6s orbitals of the gold. This results in good adsorption strength of astatine to the gold surface. This promising finding gives us a starting point towards our goal of designing an optimized gold nanoparticle for radiotherapy.

Write key words for abstract

1. Introduction

Cancer is considered insert as here one of the most deadly diseases in this world. Over 9 million people have died from cancer in the year 2020 alone.[1] Therefore, many researches are being done to treat this disease. One way in which cancer cells can be treated is by targeted α radiotherapy. Simply put, α particle emitters (isotopes that release α particles as they undergo radioactive decay) are inserted via some medium into the vicinity of the cancer cells. This allows for a localized treatment on the cancer cells.

To take advantage of this new treatment, the use of astatine in radiotherapy research has been gaining in recent years. Astatine has a shorter half-life than other α particle emitters which makes it less likely to stay active for long periods of time in the patient's body, but not so short that it is not logistically viable to be used.[2-9]

To ensure the treatment goes to the right targets, it needs to be trackable inside the body. The mechanism of labeling allows for this purpose, whereby an object (e.g. protein) is labeled (or implanted) with a radioactive substance on its surface to enable external tracking for the

said object when inserted into the test subject. In the work of Kato et al., the astatine is labeled onto gold nanoparticles of different sizes before being injected into the test subjects as α radiotherapy treatment.[2] The result is promising, as it shows the cancer cells growing much slower in the presence of the α particle treatment. Importantly, it also shows that the gold nanoparticles are able to hold onto the astatine for the duration of the testing. This presents great potential for future utilization since detached astatine particles can accumulate in other organs of the body such as the thyroid, stomach, etc. where they could cause unintended side effects[10].

Gold and, by extension, gold nanoparticles (AuNPs) have been used in applications such as electronics, catalysis, and biomedicine due to the many advantageous properties that they possess.[11-16] Synthesis of AuNPs can be tailored depending on the desired uses, and AuNPs are also deemed to be suitable for biomedical applications due to their low toxicity and ability to penetrate deep into cells.[7,9,16-21] Many applications for AuNPs have been developed including as drug carriers, tumor imaging, hyperthermia, etc.[16] AuNPs can also be used to carry out radiotherapy by being labeled with radioactive materials such as ^{225}Ac, ^{227}Th, and ^{125}I among others.[10,22,23] The additional advantage of using such methodology can be summed up in the article by Daems et al., whereby AuNPs are augmented with imaging or other treatment drugs in order to assist with the detection and/or treatment of the cancer cells.[24]

Computational Materials Design (CMD®) is a design tool developed to provide a theoretical based simulation of materials where one can tool the desired properties to match the materials' end purpose.[25] By using this method we can design an optimized AuNPs as astatine carriers for radiotherapy. Some examples of works relating to CMD® are fuel cells, hydrogen fuel storage, NO catalyst, and investigation of melanin chemistry among others.[26-30]

Previous works done in this field show that AuNPs are capable of carrying astatine to the cancer cells. However, relatively few have looked at the theoretical aspect of the adsorption of astatine on gold.[31,32] We would therefore like to establish the principles of adsorption of astatine on gold, before venturing into the task of finding the best AuNP structure and different astatine coverages to yield the most optimum result for this radioactive treatment.

2. Methodology

First principles calculation based on the density functional theory (DFT) were performed using the Vienna ab initio simulation package (VASP).[31,32] The generalized gradient approximation (GGA) with Perdew, Burke, and Ernzerhof (PBE) exchange-correlation functional was used.[33] Calculations with van der Waals interaction (vdW) utilize the DFT-D3

code based on the work done by Grimme et al.[34] The electronic one-particle wavefunctions were expanded in a plane-wave basis set up to an energy cutoff of 400 eV, while the core electrons were described by the projector augmented wave (PAW) method.[35, 36] Convergence criterion for the electronic self-consistency calculation energy is set at 10^{-5} eV and the integration for the first Brillouin zone is performed using a mesh of 5x5x1 k-points with a Monkhorst-Pack sampling scheme.[37]

The calculation model is done using a 3x3 slab of 5 layers of gold (111) separated by a vacuum of 12 Å. The bottom 2 layers are kept fixed in the bulk configuration while the top three layers are allowed to relax. A schematic of the clean Au(111) surface is shown in figure 1 with possible adsorption sites labeled.

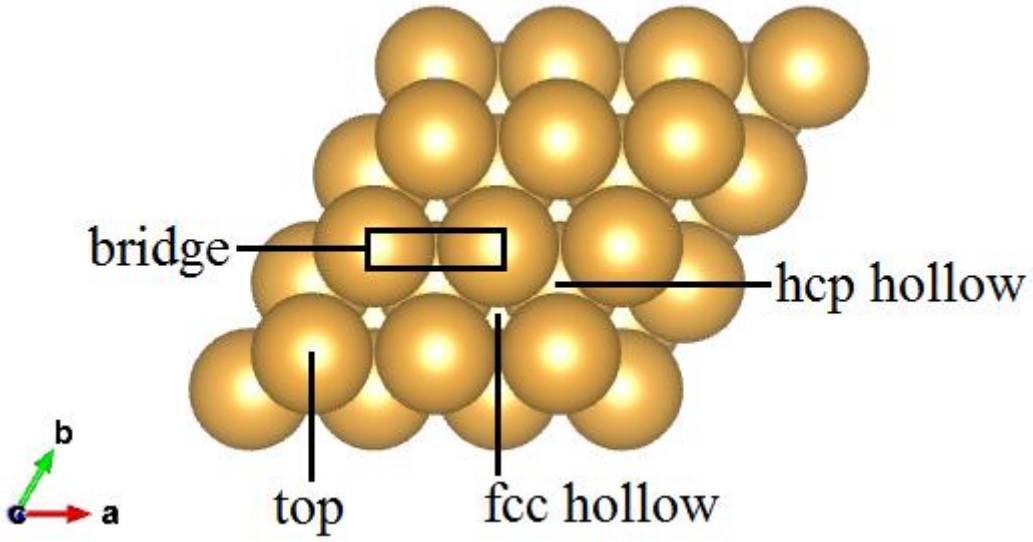

Figure 1. Adsorption sites of Au(111) surface.

The preliminary calculation to optimize the gold bulk lattice constant yields a value of 4.17 Å for non-vdW case and 4.12 Å for vdW case, both of which are in good agreement with the value of 4.0786 Å, given in the CRC Handbook of Chemistry and Physics.[38] Finally, the adsorption energies for At/Au(111) can be calculated by the equation

$$E_{bonding} = E_{At/Au(111)} - \left(0.5 \times E_{At_2}\right) - E_{Au(111)} \qquad (1)$$

where $E_{bonding}$ represents the adsorption energy, $E_{At/Au(111)}$ represents the energy of a single At atom adsorbed on Au(111) slab, E_{At_2} is the energy of the isolated At_2 molecule and $E_{Au(111)}$ is the energy of the clean Au(111) slab.

Additionally insert coma here (,) Bader charge calculations are also done to obtain the

charge transfers that happen during the adsorption process.[39] The Bader charge calculations involve only the valence electrons, since they are important in interatomic bonding, given by the electronic configurations of the two elements. The valence electrons being considered are $5d^{10}$ $6s^2$ $6p^5$ for At and $5d^{10}$ $6s^1$ for Au. For the purposes of analyzing the Bader charge calculations, negative values indicate an excess of electrons while positive values indicate a shortage of electrons.

3. Results and discussion

The molecular state of At_2 is considered as being theoretically stable. At does not exist stably in standard temperature and pressure (STP) conditions and as such the experimental data for At_2 has yet to be verified.[38] However, as reference for the adsorption energies, we believe this provides a good baseline since At is still a halogen and therefore would theoretically be most stable as a molecule. The basis for modeling nanoparticle as a slab surface comes from the findings obtained by Kleis et al.[40] The work found that as nanoparticle sizes increase above a certain threshold, the adsorption characteristics of the incoming adsorbate approaches the characteristics of that of a slab surface. This approximation allows for representation of bigger nanoparticle sizes which may contain hundreds of atoms as surface slabs and therefore removes additional burden to the computational process. It is also worth noting that for a nanoparticle, various surface facets may be present and the choice for a (111) surface is taken due to it being the most stable among the surfaces.[41,42]

The results of the adsorption energy calculations of At/Au(111) are presented in table 1, with four possible adsorption sites being considered, as shown in figure 1.

Table 1. Adsorption energies of At on different Au(111) sites.

Position	Adsorptiuon energy (w/o vdW) [eV]	Adsorption energy (w/ vdW) [eV]
Bridge	-0.854	-1.375
fcc hollow	-0.916	-1.428
hcp hollow	-0.903	-1.424
Top	-0.622	-1.204

Put straight line at the bottom to close tables in this article as indicated for this table 1.

The calculations show that the preferred site for adsorption of At is the hollow site, followed by the bridge site while the top site is less preferred for adsorption. A comparison between the calculated energies and the experiment value of -1.6 eV shows the vdW case to give a more accurate adsorption energy result compared to the non-vdW case.[31] Finally, while both hollow sites are good places for At adsorption, future calculations of At/Au(111) system will be carried out with At adsorbed on the fcc hollow site.

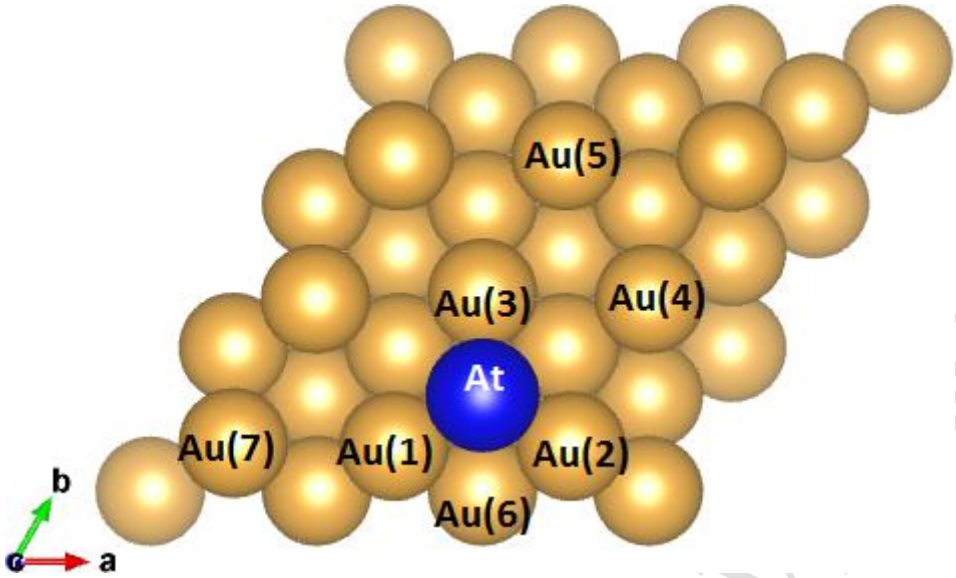

Figure 2. Schematic diagram of At on Au (111) surface.

Figure 2 shows At adsorption on Au(111) at the fcc site with labeled atoms Au(1)-Au(5) and Au(7) on the first layer (surface) and Au(6) on the second layer (first subsurface layer). Au(1), Au(2), and Au(3) are the closest Au atoms to the adsorbing At atom, and therefore represent the atoms that will directly be affected by the approach of At. Au(4), Au(5), and Au(7) are present to show the extent of the interaction due to the adsorption of At on the fcc hollow. The distances of the final adsorption configuration is given in table 2.

Table 2. Distances between selected atoms in At/Au(111) system.

Atoms	Distance (w/o vdW) [Å]	Distance (w/ vdW) [Å]
At-Au(1)		
At-Au(2)	2.962	2.952
At-Au(3)		
Au(1)-Au(2)		
Au(2)-Au(3)	3.139	3.102
Au(1)-Au(3)		
Au(3)-Au(4)	2.975	2.934
Au(4)-Au(5)	2.943	2.907
Au(1)-Au(6)	2.993	2.962
Au(2)-Au(6)		
Au(1)-Au(7)	2.854	2.819
Bulk Au	2.949	2.913

As explained earlier the vdW calculation yields a more accurate energy for the adsorption process. However, we decide to include the non-vdW calculation to look at the general trend

of adsorption between At and Au. We see an expansion of the gold atoms surrounding the fcc hollow site (Au(1)-Au(3)) possibly due to adjustment of bond length between At-Au. Both At and Au are large atoms and therefore have large atomic radii. Interestingly, this separation between the nearby gold atoms indicate that the At-Au bonding is stronger than Au-Au bonding, which further supports the adsorption energy findings.

Overall similarities between the vdW and non-vdW calculations indicate that the trend of adsorption is the increasing "hole" size around the fcc hollow due to the nearby Au atoms moving away from the At. This causes the distances of some Au atoms to reduce and therefore become constricted in movement on the surface, again supporting the earlier finding that the At-Au bonding is stronger than Au-Au bonding.

Table 3. Bader charges of At/Au(111) system.

Atom	Relative charge (before adsorption) [e/atom]	Relative charge (after adsorption) [e/atom]	Difference [e/atom]
At	0	-0.0292	-0.0292
Au(1)	0.0304	0. 0282	-0.0022
Au(2)	0.0304	0. 0269	-0.0035
Au(3)	0.0304	0.0349	0.0045
Au(4)	0.0352	0. 0196	-0.0156

Table 3 compares the results of the Bader charge calculation before and after At adsorption on Au(111) surface. The results indicate no significant difference in charges before and after the adsorption process, i.e. the electrons are shared between the At and the nearest Au atoms. At gains a slight positive charge while the charges in the Au slab are unaffected. It can be said therefore that the bonding between At and Au to be non-polar or covalent in nature.

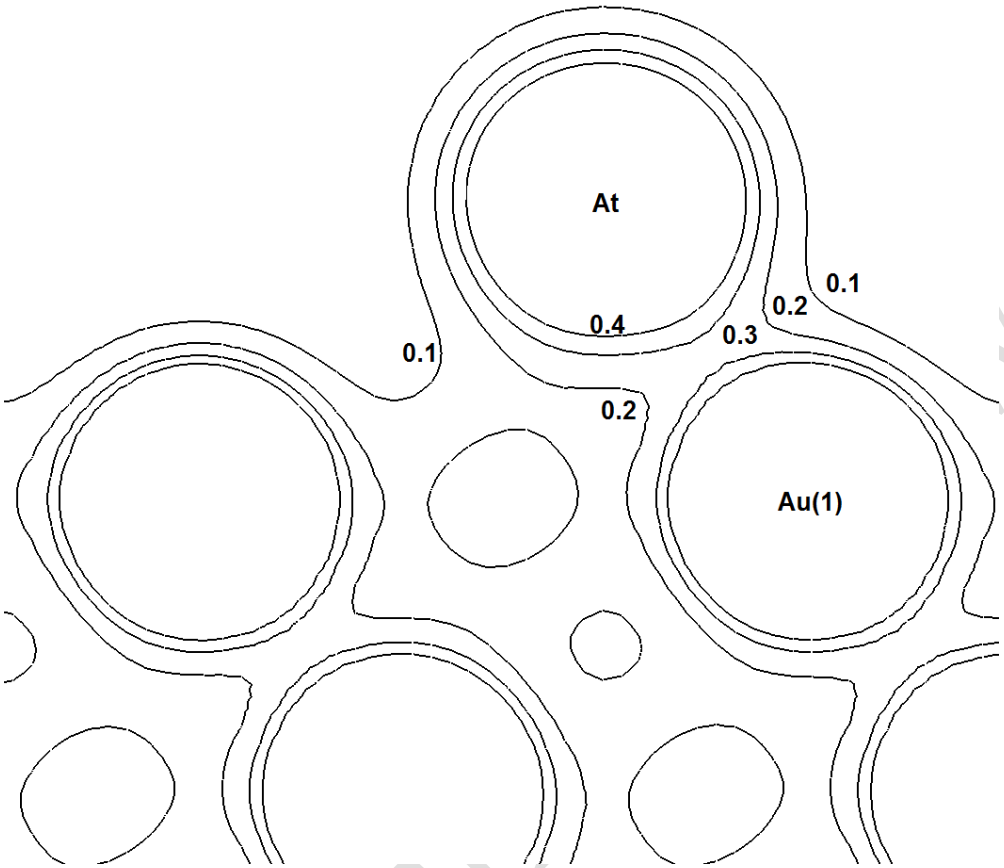

Figure 3. Charge distribution in At/Au(111) taken at the $(\bar{1}10)$ plane.

The presence of bonding can be seen in figure 3 between the At atom (topmost atom) and the neighboring Au atom (Au(1)). The lines with values on them are contour lines expressing the delineation of charge per unit volume, with 0.1 e/Å^3 intervals between each line. Only one bonding is shown since it was found that At bonded with all three nearby Au atoms and that all the bonding strengths are similar to one another. It can be seen that there is a slightly higher electron concentration between the At and Au(1), indicating that both At and the corresponding Au atoms are sharing electrons. Considering the symmetry to the other two nearest neighbors (Au(2) and Au(3)), the amount of electrons being shared is actually three times larger than what can be shown in this figure. To get a more in depth perspective, we shall look at the electronic states of the system.

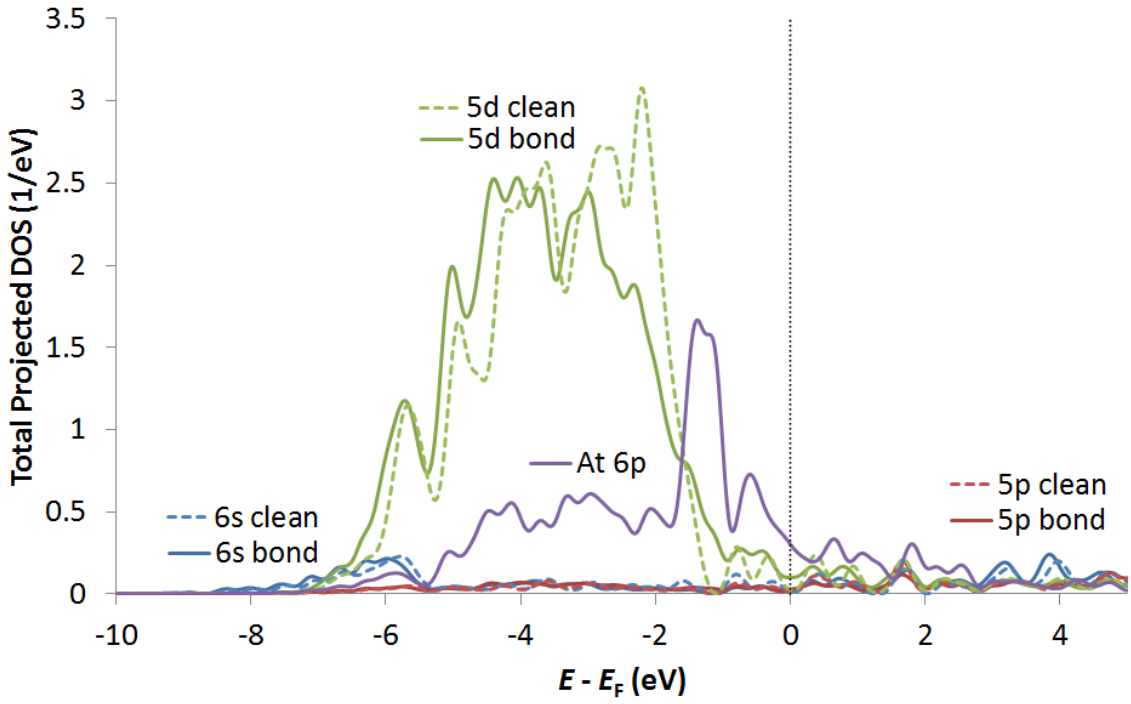

Figure 4. DOS of At/Au(111).

Figure 4 shows the density of states (DOS) of the Au(1) valence orbitals along with the At 6p orbital after adsorption. The dotted lines represent a clean Au surface (before adsorption) while the bold lines represent the Au orbitals after bonding with At (after adsorption). The purple line is the At 6p orbital after undergoing adsorption. We can see that the Au orbital changes before and after adsorption indicating the interaction between Au and At which gives rise to bonding.

Previous results have shown the bonding between At and Au to be covalent, due to the lack of charge transfer between the two elements. An indicator for this bonding is the presence of hybridization between orbitals of different reactants. In figure 4, we can see that the DOS of Au 5d "bond" orbital and the DOS of At 6p orbital are closely linked, indicating that both orbitals are affecting each other. Hybridization of the Au 5d and At 6p takes place around the -4.5 eV to -2 eV, giving rise to a higher presence of lower energy regions. These lower energy regions are occupied by the bonding electrons, providing a more stable adsorption profile for the At on Au. We also find a smaller hybridization taking place between the At 6p and Au 6s orbitals around -6 eV. These two hybridization profiles strengthen our finding that covalent bonding is the primary reason of the bonding between At and Au.

4. Conclusions

In this work, we have calculated the adsorption states of astatine on gold (111) surface to find the nature of the bonding between astatine and gold and also obtain a quantitative value for the strength of said bonding. The calculation results indicate that the astatine absorbs on hollow sites of the gold (111) surface with a relatively strong covalent bonding, caused by the hybridization of the astatine 6p orbital with the gold 5d orbital. Van der Waals interaction does not alter the characteristics of the bonding but offers more accurate adsorption energy as obtained by experiment. Understanding how astatine adsorbs on the gold (111) surface is a first step for us to construct a model by which we can experiment with other configurations and find out the relative strength of the bonding, as well as study the effect of radiation on the gold nanoparticles themselves. With this result, we hope to open a new field of application for CMD® to design optimized gold nanoparticles for the purposes of treating various cancer diseases.

References

1. (2020) [Online] International Agency for Research on Cancer: All cancers. “https://gco.iarc.fr/today/data/factsheets/cancers/39-All-cancers-fact-sheet.pdf” (Retrieved 2022-10-31).
2. H. Kato, X. Huang, Y. Kadonaga, D. Katayama, K. Ooe, A. Shimoyama, K. Kabayama, A. Toyoshima, A. Shinohara, J. Hatazawa, and K. Fukase, J. Nanobiotechnol. 19, 223 (2021).
3. G. Sgouros, J. C. Roeske, M. R. McDevitt, S. Palm, B. J. Allen, D. R. Fisher, A. Bertrand Brill, H. Song, R. W. Howell, and G Akabani, MIRD Pamphlet 22 (2010).
4. J. Elgqvist, S. Frost, J-P. Pouget, and P. Albertsson, Front. Oncol. 3, 324 (2014).
5. L. Dziawer, P. Koźmiński, S. Męczyńska-Wielgosz, M. Pruszyński, M. Łyczko, B. Wąs, G. Celichowski, J. Grobelny, J. Jastrzebski, and A. Bilewicz, RSC Adv. 7, 41024 (2017).
6. K. Kaneda-Nakashima, Z. Zhang, Y. Manabe, A. Shimoyama, K. Kabayama, T. Watabe, Y. Kanai, K. Ooe, A. Toyoshima, Y. Shirakami, T. Yoshimura, M. Fukuda, J. Hatazawa, T. Nakano, K. Fukase, and A. Shinohara, Cancer Sci. 112, 3 (2021).
7. H. Ha, H. Kwon, T. Lim, J. Jang, S. K. Park, and Y. Byun, Expert Opin. Ther. Pat. 31, 6 (2021).
8. H. K. Li, Y. Morokoshi, S. Kodaira, T. Kusumoto, K. Minegishi, H. Kanda, K. Nagatsu, and S. Hasegawa, J. Nucl. Med. 62, 11 (2021).
9. M. R. Zalutsky and M. Pruszynski, Curr. Radiopharm. 4, 3 (2011).
10. S. Poty, L. C. Francesconi, M. R. McDevitt, M. J. Morris, and J, S, Lewis, J. Nucl. Med. 59, 6

(2018).
11. D. Huang, F. Liao, S. Molesa, D. Redinger, and V. Subramanian, J. Electrochem. Soc. 150, 7 (2003).
12. M. Haruta, T. Kobayashi, H. Sano, and N. Yamada, Chem. Lett. 16, 2 (1987).
13. S. Yotsuhashi, Y. Yamada, T. Kishi, W. A. Diño, H. Nakanishi, and H. Kasai, Phys. Rev. B 77, 115413 (2008).
14. R. L. Arevalo, M. C. S. Escaño, and H. Kasai, ACS Catal. 3, 12 (2013).
15. R. L. Arevalo, S. M. Aspera, H. Nakanishi, H. Kasai, S. Yamaguchi, and K. Asazawa, Catal. Lett. 148, 1073 (2018).
16. J. Peng and X. Liang, Medicine 98, 18 (2019).
17. L. Yuan, F. Zhang, X. Qi, Y. Yang, C. Yan, J. Jiang, and J. Deng, J. Nanobiotechnol. 16, 55 (2018).
18. B. Duncan, C. Kim, and V. M. Rotello, J. Control. Release 148, 1 (2010).
19. W. H. De Jong and P. J. A. Borm, Int. J. Nanomedicine 3, 133 (2008).
20. W. Cai, T. Gao, H. Hong, and J. Sun, Nanotechnol. Sci. Appl. 1, 17 (2008).
21. A. M. Lopez-Marzo, R.Hoyos-de-la-Torre, and E. Baldrich, Anal. Chem. 90, 4010 (2018).
22. S. Poty, L. C. Francesconi, M. R. McDevitt, M. J. Morris, and J, S, Lewis, J. Nucl. Med. 59, 7 (2018).
23. A. A. Walsh, J. Nanopart. Res. 19, 152 (2017).
24. N. Daems, C. Michiels, S. Lucas, S. Baatout, and A. Aerts, Nucl. Med. Biol. 100-101, 61-90 (2021).
25. H. Kasai, H. Akai, and H. Yoshida, *Computational Materials Design from Basics to Actual Applications* (Osaka University Press, Suita, Japan, 2005) (in Japanese).
26. H. Kasai and M. Tsuda, *Computational Materials Design, Case Study I: Intelligent/Directed Materials Design for Polymer Electrolyte Fuel Cells and Hydrogen Storage Applications* (Osaka University Press, Suita, Japan, 2008) (in Japanese).
27. H. Kasai, and M. C. S. Escaño, Eds.: *Physics of Surface, Interface, and Cluster Catalysis* (IOP Publishing Bristol UK, 2016).
28. H. Kasai, A. A. B. Padama, B. Chantaramolee, and R. L. Arevalo, *Hydrogen and Hydrogen-Containing Molecules on Metal Surfaces* (Springer, Singapore, 2020).
29. S. M. Aspera, R. L. Arevalo, B. Chantaramolee, H. Nakanishi, and H. Kasai, Phys. Chem. Chem. Phys. 23, 7153-7163 (2021).
30. R. Kishida, S. M. Aspera, and H. Kasai, *Melanin Chemistry Explored by Quantum Mechanics* (Springer, Singapore, 2021).
31. A. Serov, N. Aksenov, G. Bozhikov, R. Eichler, R. Dressler, V. Lebedev, O. Petrushkin, D. Piguet, S. Shishkin, E. Tereshatov, A. Türler, A. Vögele, D. Wittwer, and H. W. Gäggeler, Radiochim. Acta 99, 593-599 (2011).
32. Y. Demidov and A. Zaitsevskii, Chem. Phys. Lett. 691, 126-130 (2018).

33. G. Kresse and J. Furthmüller, Phys. Rev. B 54, 11169 (1996).
34. G. Kresse and J. Furthmüller, Comput. Mater. Sci. B 6, 15 (1996).
35. J. P. Perdew, K. Burke, and M. Ernzerhof, Phys. Rev. Lett. 77, 3865 (1996).
36. S. Grimme, S. Ehrlich, and L. Goerigk, J. Comput. Chem. 32, 1456 (2011).
37. P. E. Blöchl, Phys. Rev. B: Condens. Matter Mater. Phys. 50, 17953 (1994).
38. G. Kresse and D. Joubert, Phys. Rev. B: Condens. Matter Mater. Phys. 59, 1759 (1999).
39. H. J. Monkhorst and J. D. Pack, Phys. Rev. B: Condens. Matter Mater. Phys. 13, 12 (1976).
40. D. R. Lide, Ed.: *CRC Handbook of Chemistry and Physics* (Taylor & Francis Group, Florida, 2005) 86th ed., p. 4-5.
41. G. Henkelman, A. Arnaldson, and H. Jónsson, Comput. Mater. Sci. 36, 254 (2006).
42. J. Kleis, J. Greeley, N. A. Romero, V. A. Morozov, H. Falsig, A. H. Larsen, J. Lu, J. J. Mortensen, M. Dulak, K. S. Thygesen, J. K. Norskøv, and K. J. Jacobsen, Catal. Lett. 141, 1067 (2011).
43. G. Grochola, I. K. Snook, and S. P. Russo, J. Chem. Phys. 127, 224704 (2007).
44. D. Holec, P. Dumitraschkewitz, D. Vollath, and F. D. Fischer, Nanomaterials 10, 484 (2020).